

An Energy Stable One-Field Fictitious Domain Method for Fluid-Structure Interactions

Yongxing Wang*, Peter K. Jimack, Mark A. Walkley

School of Computing, University of Leeds, Leeds, UK, LS2 9JT

Abstract

In this article, the energy stability of a one-field fictitious domain method is proved and validated by numerical tests in two and three dimensions. The distinguishing feature of this method is that it only solves for one velocity field for the whole fluid-structure domain; the interactions remain decoupled until solving the final linear algebraic equations. To achieve this the finite element procedures are carried out separately on two different meshes for the fluid and solid respectively, and the assembly of the final linear system brings the fluid and solid parts together via an isoparametric interpolation matrix between the two meshes. The weak formulations are introduced in the continuous case and after discretization in time. Then the stability is analyzed through an energy estimate. Finally, numerical examples are presented to validate the energy stability properties.

Keywords: Fluid-Structure Interactions, Fictitious Domain Method, One-Field Fictitious Domain Method, Energy Stable Scheme.

1. Introduction

Three major questions arise when considering a finite element method for the problem of Fluid-Structure Interactions (FSI): (1) what kind of meshes are used (interface fitted or unfitted); (2) how to couple the fluid-structure interactions (monolithic/fully-coupled or partitioned/segregated); (3) what variables are solved (velocity and/or displacement). Combinations of the answers of these questions lead to different types of numerical method. For example, [1, 2] solve for fluid velocity and solid displacement sequentially (partitioned/segregated) using an Arbitrary Lagrangian-Eulerian (ALE) fitted mesh, whereas [3–5] use an ALE fitted mesh to solve for fluid velocity and solid displacement simultaneously (monolithic/fully-coupled) with a Lagrange Multiplier to enforce the continuity of velocity/displacement on the interface. The Immersed Finite Element Method (IFEM) [6–12] and the Fictitious Domain Method (FDM) [13–18]

*Corresponding author

Email address: jungsirwang@gmail.com/scywa@leeds.ac.uk (Yongxing Wang)

use two meshes to represent the fluid and solid separately. Although IFEM
 15 could be monolithic [6], the classical IFEM only solves for velocity, while the
 solid information is arranged on the right-hand side of the fluid equation as a
 prescribed force term. Although the FDM may be partitioned [18], usually the
 FDM approach solves for both velocity in the whole domain (fluid plus solid) and
 displacement of the solid simultaneously via a distributed Lagrange multiplier
 20 (DLM) to enforce the consistency of velocity/displacement in the overlapped
 solid domain. In the case of one-field and monolithic numerical methods for FSI
 problems, [19] introduces a 1D model using a one-field FDM formulation based
 on two meshes, and [20, 21] introduces an energy stable monolithic method (in
 2D) based on one Eulerian mesh and discrete remeshing.

25 In a previous study [22], we present a one-field monolithic fictitious domain
 method (subsequently referred to as the one-field FDM) which has the following
 main features: (1) only one velocity field is solved in the whole domain, based
 upon the use of an appropriate L^2 projection; (2) the fluid and solid equations
 are solved monolithically. Our motivation for proposing the one-field FDM is
 30 based on comparing its features with those of existing numerical schemes. Com-
 pared with IFEM the classical IFEM does not solve the solid equation [8–12].
 Instead, the solid information is arranged on the right-hand side of the fluid
 equation as a prescribed force. The one-field FDM solves the solid equation
 together with the fluid equation in one discretized linear algebraic system. The
 35 similarity is that both methods only solve for velocity and pressure fields (no
 solid displacement). DLM/FDM methods [13–18] solve the solid equation, but
 for a displacement field, and couple this displacement with the velocity of the
 fictitious fluid via a Lagrange multiplier. This leads to a large discretized lin-
 ear algebra system. The one-field FDM rewrites the solid equation in terms
 40 of a velocity variable and couples the fictitious fluid through a finite element
 interpolation. Monolithic Eulerian methods [20, 21] also express the solid equa-
 tion in terms of velocity, and the fluid and solid are coupled naturally on an
 interface-fitted mesh. The one-field FDM uses two meshes to represent the fluid
 and solid respectively. Consequently, before discretization in space, these two
 45 methods have many similarities, the advantage of the one-field FDM being that
 interface fitting is not required.

The main developments in this paper, following from [22], are as follows.
 The energy preserving property in the continuous case is proved. The energy
 nonincreasing property after time discretization is proved, and the same prop-
 50 erty is also proved after spatial discretization. The implementation in this paper
 is based on an \mathbf{F} -scheme, i.e., the solid deformation tensor \mathbf{F} is updated (see
 section 4), while the previous paper uses a $\boldsymbol{\sigma}$ -scheme (see equation (29) in [22]).
 The advantage of this \mathbf{F} -scheme is that the integral is expressed in the refer-
 ence domain so that it becomes linear for the neo-Hookean solid model (see
 55 equation (15)), which however is nonlinear if expressed in the current domain
 for the $\boldsymbol{\sigma}$ -scheme (see equation (29) in [22]). The methodology and analysis is
 demonstrated to extend to the three-dimensional case.

The paper is organized as follows. Control equations and weak formulation
 are introduced in section 2 and 3 respectively. The time discretized weak form

60 is then presented in section 4. Stability of the proposed scheme is analyzed in
 section 5. Space discretization is discussed in section 6. Numerical examples
 are given in section 7, and conclusions are presented in section 8.

2. Control equations

65 In the following context, $\Omega_t^f \subset \mathbb{R}^d$ and $\Omega_t^s \subset \mathbb{R}^d$ with $d = 2, 3$ denote the
 fluid and solid domain respectively which are time dependent regions as shown
 in Figure 1. $\Omega = \Omega_t^f \cup \Omega_t^s$ is a fixed domain (with outer boundary Γ) and
 $\Gamma_t = \partial\Omega_t^f \cap \partial\Omega_t^s$ is the moving interface between fluid and solid. We denote by
 \mathbf{X} the reference (material) coordinates of the solid, by $\mathbf{x} = \mathbf{x}(\cdot, t)$ the current
 coordinates of the solid, and by \mathbf{x}_0 the initial coordinates of the solid.

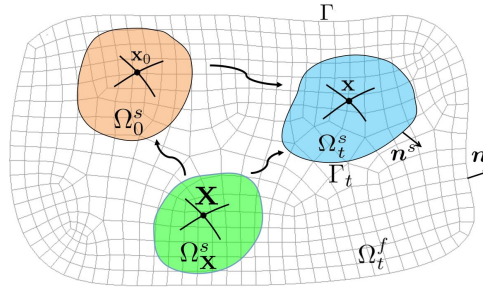


Figure 1: Schematic diagram of FSI, $\Omega = \Omega_t^f \cup \Omega_t^s$.

70 Let $\rho, \mu, \mathbf{u}, p, \boldsymbol{\sigma}$ denote the density, viscosity, velocity, pressure and stress
 tensor respectively. We assume both an incompressible fluid and incompressible
 solid, then the conservation of momentum and conservation of mass take the
 same form as follows:

Momentum equation:

$$\rho \frac{d\mathbf{u}}{dt} = \nabla \cdot \boldsymbol{\sigma}, \quad (1)$$

Continuity equation:

$$\nabla \cdot \mathbf{u} = 0. \quad (2)$$

An incompressible Newtonian constitutive equation in Ω^f can be expressed
 as:

$$\boldsymbol{\sigma} = \boldsymbol{\sigma}^f = \mu^f \mathbf{D}\mathbf{u}^f - p^f \mathbf{I}, \quad (3)$$

where $\mathbf{D}\mathbf{u} = \nabla \mathbf{u} + \nabla^T \mathbf{u}$. We shall use an incompressible neo-Hookean solid in
 Ω_t^s [14, 20], and in common with previous work [10, 12] we also assume the solid
 has the same viscosity as the fluid. The constitutive equation may be expressed
 as:

$$\boldsymbol{\sigma} = \boldsymbol{\sigma}^s = c_1 J^{-1} (\mathbf{F}\mathbf{F}^T - \mathbf{I}) + \mu^s \mathbf{D}\mathbf{u}^s - p^s \mathbf{I}, \quad (4)$$

where $\mathbf{F} = \frac{\partial \mathbf{x}}{\partial \mathbf{X}} = \frac{\partial \mathbf{x}}{\partial \mathbf{x}_0} \frac{\partial \mathbf{x}_0}{\partial \mathbf{X}} = \nabla_0 \mathbf{x} \nabla_{\mathbf{X}} \mathbf{x}_0$ is the deformation tensor of the solid, and
 $J = \det \mathbf{F}$ is the determinant of \mathbf{F} . Finally the system is complemented with the

following boundary and initial conditions.

$$\mathbf{u}^f = \mathbf{u}^s \quad \text{on} \quad \Gamma_t, \quad (5)$$

$$\mathbf{n}^s \boldsymbol{\sigma}^f = \mathbf{n}^s \boldsymbol{\sigma}^s \quad \text{on} \quad \Gamma_t, \quad (6)$$

$$\mathbf{u}^f = \mathbf{0} \quad \text{on} \quad \Gamma, \quad (7)$$

$$\mathbf{u}^f|_{t=0} = \mathbf{u}_0^f, \quad (8)$$

$$\mathbf{u}^s|_{t=0} = \mathbf{u}_0^s. \quad (9)$$

Other boundary conditions are possible on Γ but (7) are used here for simplicity.

Remark 1. *The corresponding energy function for the hyperelastic stress in (4) is defined by [16]:*

$$\Psi(\mathbf{F}) = \frac{c_1}{2} (\text{tr}_{\mathbf{F}\mathbf{F}^T} - d) - c_1 \ln(J). \quad (10)$$

75 3. Weak formulation

The finite element weak form discussed in this section is almost the same as that in [22], the only difference is that we integrate the solid stress in the reference domain, because we shall update the deformation tensor (\mathbf{F} -scheme) rather than the solid stress as done in [22] ($\boldsymbol{\sigma}$ -scheme). In the following context, let $L^2(\omega)$ be the square integrable functions in domain ω , endowed with norm $\|u\|_{0,\omega}^2 = \int_{\omega} |u|^2$ ($u \in L^2(\omega)$). Let $H^1(\omega) = \{u : u, \nabla u \in L^2(\omega)\}$ with the norm denoted by $\|u\|_{1,\omega}^2 = \|u\|_{0,\omega}^2 + \|\nabla u\|_{0,\omega}^2$. We also denote by $H_0^1(\omega)$ the subspace of $H^1(\omega)$ whose functions have zero values on the boundary of ω , and denote by $L_0^2(\omega)$ the subspace of $L^2(\omega)$ whose functions have zero mean value.

Let $p = \begin{cases} p^f & \text{in} \quad \Omega_t^f \\ p^s & \text{in} \quad \Omega_t^s \end{cases}$. Given $\mathbf{v} \in H_0^1(\Omega)^d$, we perform the following symbolic operations:

$$\int_{\Omega_t^f} \text{Eq.(1)} \cdot \mathbf{v} d\mathbf{x} + \int_{\Omega_t^s} \text{Eq.(1)} \cdot \mathbf{v} d\mathbf{x}.$$

Integrating the stress terms by parts, the above operations, using constitutive equation (3) and (4) and boundary condition (6), gives:

$$\begin{aligned} & \rho^f \int_{\Omega} \frac{d\mathbf{u}}{dt} \cdot \mathbf{v} d\mathbf{x} + \frac{\mu^f}{2} \int_{\Omega} \mathbf{D}\mathbf{u} : \mathbf{D}\mathbf{v} d\mathbf{x} - \int_{\Omega} p \nabla \cdot \mathbf{v} d\mathbf{x} \\ & + \rho^s \int_{\Omega_t^s} \frac{d\mathbf{u}}{dt} \cdot \mathbf{v} d\mathbf{x} + c_1 \int_{\Omega_t^s} J^{-1} (\mathbf{F}\mathbf{F}^T - \mathbf{I}) : \nabla \mathbf{v} d\mathbf{x} = 0, \end{aligned} \quad (11)$$

85 where $\rho^\delta = \rho^s - \rho^f$. Note that the integrals on the interface Γ_t are cancelled out using boundary condition (6). This is not surprising because they are internal forces for the whole FSI system considered here.

Transforming the integral of the last two terms of (11) to the reference coordinate system, combined with the following symbolic operations for $q \in L^2(\Omega)$,

$$-\int_{\Omega_t^f} \text{Eq.}(2)q d\mathbf{x} - \int_{\Omega_t^s} \text{Eq.}(2)q d\mathbf{x},$$

leads to the weak form of the FSI system as follows.

Problem 1. Given \mathbf{u}_0 and Ω_0^s , find $\mathbf{u}(t) \in H_0^1(\Omega)^d$, $p(t) \in L_0^2(\Omega)$ and Ω_t^s , such that for $\forall \mathbf{v} \in H_0^1(\Omega)^d$, $\forall q \in L^2(\Omega)$, the following two equations hold:

$$\begin{aligned} & \rho^f \int_{\Omega} \frac{\partial \mathbf{u}}{\partial t} \cdot \mathbf{v} d\mathbf{x} + \rho^f \int_{\Omega} (\mathbf{u} \cdot \nabla) \mathbf{u} \cdot \mathbf{v} d\mathbf{x} + \frac{\mu^f}{2} \int_{\Omega} \mathbf{D}\mathbf{u} : \mathbf{D}\mathbf{v} d\mathbf{x} - \int_{\Omega} p \nabla \cdot \mathbf{v} d\mathbf{x} \\ & + \rho^\delta \int_{\Omega_{\mathbf{x}}^s} \frac{\partial \mathbf{u}}{\partial t} \cdot \mathbf{v} d\mathbf{X} + c_1 \int_{\Omega_{\mathbf{x}}^s} \mathbf{F} : \nabla_{\mathbf{x}} \mathbf{v} d\mathbf{X} - c_1 \int_{\Omega_t^s} J^{-1} \nabla \cdot \mathbf{v} d\mathbf{x} = 0, \end{aligned} \quad (12)$$

and

$$-\int_{\Omega} q \nabla \cdot \mathbf{u} d\mathbf{x} = 0. \quad (13)$$

90 **Remark 2.** Because domain Ω is stationary (the Eulerian description will be used) and Ω_t^s is transient which will be updated by its own velocity (the updated Lagrangian description), there is a convection term from the total derivative of time in Ω , but there is no convection term in Ω_t^s .

Remark 3. Problem 1 is equivalent to the equation (12) in [22].

4. Discretization in time

We may use the backward Euler method to discretize Problem 1, and update coordinates of the solid by $\mathbf{x}_{n+1} = \mathbf{x}_n + \Delta t \mathbf{u}_{n+1}$. As a result, \mathbf{F} is updated by $\mathbf{F}_{n+1} = \mathbf{F}_n + \Delta t \nabla_{\mathbf{x}} \mathbf{u}_{n+1}$, and so,

$$\int_{\Omega_{\mathbf{x}}^s} \mathbf{F}_{n+1} : \nabla_{\mathbf{x}} \mathbf{v} = \int_{\Omega_{\mathbf{x}}^s} \mathbf{F}_n : \nabla_{\mathbf{x}} \mathbf{v} + \Delta t \int_{\Omega_{\mathbf{x}}^s} \nabla_{\mathbf{x}} \mathbf{u}_{n+1} : \nabla_{\mathbf{x}} \mathbf{v}. \quad (14)$$

95 Using equation (14), the discretized weak form corresponding to Problem 1 may be expressed as:

Problem 2. Given \mathbf{u}_n , p_n and Ω_n^s , find $\mathbf{u}_{n+1} \in H_0^1(\Omega)^d$, $p_{n+1} \in L_0^2(\Omega)$ and Ω_{n+1}^s , such that for $\forall \mathbf{v} \in H_0^1(\Omega)^d$, $\forall q \in L^2(\Omega)$, the following four relations

hold:

$$\begin{aligned}
& \rho^f \int_{\Omega} \frac{\mathbf{u}_{n+1} - \mathbf{u}_n}{\Delta t} \cdot \mathbf{v} d\mathbf{x} + \rho^f \int_{\Omega} (\mathbf{u}_{n+1} \cdot \nabla) \mathbf{u}_{n+1} \cdot \mathbf{v} d\mathbf{x} \\
& + \frac{\mu^f}{2} \int_{\Omega} \mathbf{D}\mathbf{u}_{n+1} : \mathbf{D}\mathbf{v} d\mathbf{x} - \int_{\Omega} p_{n+1} \nabla \cdot \mathbf{v} d\mathbf{x} \\
& + \rho^\delta \int_{\Omega_{\mathbf{x}}^s} \frac{\mathbf{u}_{n+1} - \mathbf{u}_n}{\Delta t} \cdot \mathbf{v} d\mathbf{X} + c_1 \Delta t \int_{\Omega_{\mathbf{x}}^s} \nabla_{\mathbf{X}} \mathbf{u}_{n+1} : \nabla_{\mathbf{X}} \mathbf{v} d\mathbf{X} \\
& - c_1 \int_{\Omega_{n+1}^s} J_{n+1}^{-1} \nabla \cdot \mathbf{v} d\mathbf{x} = -c_1 \int_{\Omega_{\mathbf{x}}^s} \mathbf{F}_n \nabla_{\mathbf{X}} \mathbf{v} d\mathbf{X}, \\
& - \int_{\Omega} q \nabla \cdot \mathbf{u}_{n+1} d\mathbf{x} = 0,
\end{aligned} \tag{15}$$

$$\Omega_{n+1}^s = \{\mathbf{x} : \mathbf{x} = \mathbf{x}_n + \Delta t \mathbf{u}_{n+1}, \mathbf{x}_n \in \Omega_n^s\}, \tag{17}$$

and

$$\mathbf{F}_{n+1} = \mathbf{F}_n + \Delta t \nabla_{\mathbf{X}} \mathbf{u}_{n+1}. \tag{18}$$

Remark 4. We shall use a fixed-point iteration at each time step to construct Ω_{n+1}^s implicitly.

Remark 5. Problem 2 is similar to equation (30) in [22], however here the discretized weak form is expressed as an implicit scheme, and the solid deformation tensor \mathbf{F} is updated rather than the solid stress $\boldsymbol{\sigma}^s$ in [22].

5. Stability by energy estimate

5.1. Energy conservation in the continuous case

In this section we shall prove that the weak forms (12) and (13), associated with Problem 1, preserve energy.

Lemma 3. The energy function $\Psi(\mathbf{F})$ for the hyperelastic stress satisfies:

$$c_1 \int_0^t \int_{\Omega_{\mathbf{x}}^s} \mathbf{F} : \nabla_{\mathbf{X}} \mathbf{u} d\mathbf{X} - c_1 \int_0^t \int_{\Omega_t^s} J^{-1} \nabla \cdot \mathbf{u} d\mathbf{x} = \int_{\Omega_{\mathbf{x}}^s} \Psi(\mathbf{F}) d\mathbf{X}. \tag{19}$$

Proof. Since $\frac{\partial \text{tr}_{\mathbf{F}\mathbf{F}^T}}{\partial \mathbf{F}} = 2\mathbf{F}$ and $\frac{\partial(\det \mathbf{F})}{\partial \mathbf{F}} = \det \mathbf{F} \mathbf{F}^{-T}$. Using the fact that $\mathbf{A} : \mathbf{B} = \text{tr}_{\mathbf{A}\mathbf{B}^T}$ (\mathbf{A} and \mathbf{B} are arbitrary matrices), we have:

$$\begin{aligned}
& \frac{d}{dt} \int_{\Omega_{\mathbf{x}}^s} \Psi(\mathbf{F}) d\mathbf{X} = \int_{\Omega_{\mathbf{x}}^s} \frac{\partial \Psi}{\partial \mathbf{F}} : \frac{d\mathbf{F}}{dt} d\mathbf{X} \\
& = c_1 \int_{\Omega_{\mathbf{x}}^s} (\mathbf{F} - \mathbf{F}^{-T}) : \frac{d}{dt} (\mathbf{I} + \nabla_{\mathbf{X}} \mathbf{d}) d\mathbf{X} \\
& = c_1 \int_{\Omega_{\mathbf{x}}^s} \mathbf{F} : \nabla_{\mathbf{X}} \mathbf{u} d\mathbf{X} - c_1 \int_{\Omega_t^s} J^{-1} \nabla \cdot \mathbf{u} d\mathbf{x},
\end{aligned}$$

where \mathbf{d} is displacement of the solid at time t . □

Lemma 4. *If (\mathbf{u}, p) is the solution pair of Problem 1, then*

$$\int_{\Omega} (\mathbf{u} \cdot \nabla) \mathbf{u} \cdot \mathbf{u} d\mathbf{x} = 0. \quad (20)$$

Proof. First,

$$\int_{\Omega} (\mathbf{u} \cdot \nabla) \mathbf{u} \cdot \mathbf{u} d\mathbf{x} = \int_{\Omega} \nabla (\mathbf{u} \otimes \mathbf{u}) \cdot \mathbf{u} d\mathbf{x} - \int_{\Omega} |\mathbf{u}|^2 \nabla \cdot \mathbf{u} d\mathbf{x}. \quad (21)$$

Integrate by parts:

$$\int_{\Omega} \nabla (\mathbf{u} \otimes \mathbf{u}) \cdot \mathbf{u} d\mathbf{x} = \int_{\Gamma} |\mathbf{u}|^2 \mathbf{u} \cdot \mathbf{n} d\Gamma - \int_{\Omega} (\mathbf{u} \cdot \nabla) \mathbf{u} \cdot \mathbf{u} d\mathbf{x}. \quad (22)$$

According to a Sobolev imbedding theorem [23, Theorem 6 in Chapter 5] and the inclusion between L^p spaces ($L^q \subset L^p$ if $p < q$), we know $H^1(\Omega) \subset L^4(\Omega)$ (for both 2D and 3D). Therefore $\mathbf{u} \in L^4(\Omega)$, i.e., $\int_{\Omega} |\mathbf{u}|^4 d\mathbf{x} < \infty$. That is to say $|\mathbf{u}|^2 \in L^2(\Omega)$. Then we have $\int_{\Omega} |\mathbf{u}|^2 \nabla \cdot \mathbf{u} = 0$ from (13). We also have $\int_{\Gamma} |\mathbf{u}|^2 \mathbf{u} \cdot \mathbf{n} = 0$ from the boundary condition (7). Substituting these two equations into (21) and (22) gives equation (20). \square

Proposition 5 (Energy Conservation). *Let (\mathbf{u}, p) be the solution pair of Problem 1, then*

$$\begin{aligned} & \frac{\rho^f}{2} \int_{\Omega} |\mathbf{u}|^2 d\mathbf{x} + \frac{\mu^f}{2} \int_0^t \int_{\Omega} \mathbf{D}\mathbf{u} : \mathbf{D}\mathbf{u} d\mathbf{x} \\ & + \frac{\rho^\delta}{2} \int_{\Omega_{\mathbf{x}}^\delta} |\mathbf{u}|^2 d\mathbf{X} + \int_{\Omega_{\mathbf{x}}^\delta} \Psi(\mathbf{F}) d\mathbf{X} = \mathbf{0}. \end{aligned} \quad (23)$$

Proof. We first let $\mathbf{v} = \mathbf{u}$ in (12) and integrate from time 0 to t , then let $q = p$ in (13) and substitute into (12). Finally we can construct the above equation of energy balance due to Lemma 3 and 4. \square

5.2. Stability analysis after time discretization

We next demonstrate a similar energy stability result for Problem 2.

Lemma 6. *The trace function $\frac{1}{2} \text{tr}(\mathbf{F}\mathbf{F}^T)$ satisfies:*

$$\frac{1}{2} \text{tr}(\mathbf{F}_{n+1} \mathbf{F}_{n+1}^T) - \frac{1}{2} \text{tr}(\mathbf{F}_n \mathbf{F}_n^T) = \Delta t \mathbf{F}_{n+1} : \nabla_{\mathbf{X}} \mathbf{u}_{n+1} - \frac{\Delta t^2}{2} |\nabla_{\mathbf{X}} \mathbf{u}_{n+1}|^2, \quad (24)$$

where $|\mathbf{A}|^2 = \sum_{ij} a_{ij}^2$ for an arbitrary matrix $\mathbf{A} = [a_{ij}]$.

Proof.

$$\begin{aligned} & \mathbf{F}_{n+1} \mathbf{F}_{n+1}^T - \mathbf{F}_n \mathbf{F}_n^T \\ & = \mathbf{F}_{n+1} \mathbf{F}_{n+1}^T - (\mathbf{F}_{n+1} - \Delta t \nabla_{\mathbf{X}} \mathbf{u}_{n+1}) (\mathbf{F}_{n+1} - \Delta t \nabla_{\mathbf{X}} \mathbf{u}_{n+1})^T \\ & = \Delta t \mathbf{F}_{n+1} \nabla_{\mathbf{X}}^T \mathbf{u}_{n+1} + \Delta t \nabla_{\mathbf{X}} \mathbf{u}_{n+1} \mathbf{F}_{n+1}^T - \Delta t^2 \nabla_{\mathbf{X}} \mathbf{u}_{n+1} \nabla_{\mathbf{X}}^T \mathbf{u}_{n+1}. \end{aligned}$$

Lemma 6 holds due to

$$\frac{1}{2} \text{tr}(\mathbf{F}_{n+1}\mathbf{F}_{n+1}^T - \mathbf{F}_n\mathbf{F}_n^T) = \Delta t \cdot \text{tr}(\mathbf{F}_{n+1}\nabla_{\mathbf{X}}^T \mathbf{u}_{n+1}) - \frac{\Delta t^2}{2} |\nabla_{\mathbf{X}} \mathbf{u}_{n+1}|^2.$$

□

Lemma 7. *The log-determinant function $\ln(\det \mathbf{F})$ satisfies:*

$$\ln(\det \mathbf{F}_{n+1}) - \ln(\det \mathbf{F}_n) \geq \Delta t \nabla \cdot \mathbf{u}_{n+1} - \frac{\Delta t^2}{2} |\mathbf{F}_{n+1}^{-1} \nabla_{\mathbf{X}} \mathbf{u}_{n+1}|^2.$$

Proof. Use the fact that function $\ln(\det \mathbf{Y})$ is concave over the set of positive definite matrices [24, Chapter 3]. Let $\mathbf{B} = \mathbf{F}\mathbf{F}^T$, $\mathcal{F}(\mathbf{B}) = \frac{1}{2} \ln(\det \mathbf{B}) = \ln(\det \mathbf{F})$ and $w(\xi) = \mathcal{F}(\mathbf{B}_n + \xi(\mathbf{B}_{n+1} - \mathbf{B}_n))$, then

$$w'(\xi) = \frac{d\mathcal{F}}{d\mathbf{B}} : (\mathbf{B}_{n+1} - \mathbf{B}_n) = \frac{1}{2} (\mathbf{B}_n + \xi(\mathbf{B}_{n+1} - \mathbf{B}_n))^{-1} : (\mathbf{B}_{n+1} - \mathbf{B}_n).$$

According to the property of concave functions, we have $w(1) - w(0) \geq w'(1)$, this is to say:

$$\begin{aligned} \ln(\det \mathbf{F}_{n+1}) - \ln(\det \mathbf{F}_n) &= \mathcal{F}(\mathbf{B}_{n+1}) - \mathcal{F}(\mathbf{B}_n) \\ &\geq \frac{1}{2} \mathbf{B}_{n+1}^{-1} : (\mathbf{B}_{n+1} - \mathbf{B}_n) = \frac{1}{2} \text{tr}(\mathbf{I} - \mathbf{B}_{n+1}^{-1} \mathbf{B}_n) \\ &= \frac{1}{2} \text{tr}(\mathbf{I} - \mathbf{B}_{n+1}^{-1} (\mathbf{F}_{n+1} - \Delta t \nabla_{\mathbf{X}} \mathbf{u}_{n+1}) (\mathbf{F}_{n+1}^T - \Delta t \nabla_{\mathbf{X}}^T \mathbf{u}_{n+1})) \\ &= \frac{\Delta t}{2} \text{tr}(\mathbf{F}_{n+1}^{-T} \nabla_{\mathbf{X}}^T \mathbf{u}_{n+1} + \mathbf{F}_{n+1}^{-T} \mathbf{F}_{n+1}^{-1} \nabla_{\mathbf{X}} \mathbf{u}_{n+1} \mathbf{F}_{n+1}^T) \\ &\quad - \frac{\Delta t^2}{2} \text{tr}(\mathbf{F}_{n+1}^{-T} \mathbf{F}_{n+1}^{-1} \nabla_{\mathbf{X}} \mathbf{u}_{n+1} \nabla_{\mathbf{X}}^T \mathbf{u}_{n+1}) \\ &= \Delta t \nabla \cdot \mathbf{u}_{n+1} - \frac{\Delta t^2}{2} |\mathbf{F}_{n+1}^{-1} \nabla_{\mathbf{X}} \mathbf{u}_{n+1}|^2. \end{aligned}$$

¹²⁰ In the above, we use the trace property of cyclic permutations: $\text{tr}(\mathbf{A}_1 \mathbf{A}_2 \mathbf{A}_3) = \text{tr}(\mathbf{A}_2 \mathbf{A}_3 \mathbf{A}_1) = \text{tr}(\mathbf{A}_3 \mathbf{A}_1 \mathbf{A}_2)$. □

From the above two lemmas, we have:

Proposition 8. *The energy function $\Psi(\mathbf{F})$ for the hyperelastic stress satisfies:*

$$\begin{aligned} &\int_{\Omega_{\mathbf{X}}^s} \Psi(\mathbf{F}_{n+1}) d\mathbf{X} - \int_{\Omega_{\mathbf{X}}^s} \Psi(\mathbf{F}_n) d\mathbf{X} \\ &\leq \Delta t c_1 \int_{\Omega_{\mathbf{X}}^s} \mathbf{F}_{n+1} : \nabla_{\mathbf{X}} \mathbf{u}_{n+1} d\mathbf{X} - \Delta t c_1 \int_{\Omega_{n+1}^s} J_{n+1}^{-1} \nabla \cdot \mathbf{u}_{n+1} d\mathbf{x} + R_{n+1}, \end{aligned} \quad (25)$$

where

$$R_{n+1} = \frac{c_1 \Delta t^2}{2} \int_{\Omega_{\mathbf{X}}^s} \left(|\mathbf{F}_{n+1}^{-1} \nabla_{\mathbf{X}} \mathbf{u}_{n+1}|^2 - |\nabla_{\mathbf{X}} \mathbf{u}_{n+1}|^2 \right) d\mathbf{X}. \quad (26)$$

Similarly to Lemma 4, we have:

Lemma 9. *If $(\mathbf{u}_{n+1}, p_{n+1})$ is the solution pair of Problem 2, then*

$$\int_{\Omega} (\mathbf{u}_{n+1} \cdot \nabla) \mathbf{u}_{n+1} \cdot \mathbf{u}_{n+1} d\mathbf{x} = 0. \quad (27)$$

Proposition 10 (Energy Nonincreasing). *Let $(\mathbf{u}_{n+1}, p_{n+1})$ be the solution pair of Problem 2. If $\rho^\delta \geq 0$, then*

$$\begin{aligned} & \frac{\rho^f}{2} \int_{\Omega} |\mathbf{u}_{n+1}|^2 d\mathbf{x} + \frac{\rho^\delta}{2} \int_{\Omega_{\mathbf{x}}^s} |\mathbf{u}_{n+1}|^2 d\mathbf{X} + \int_{\Omega_{\mathbf{x}}^s} \Psi(\mathbf{F}_{n+1}) d\mathbf{X} \\ & + \frac{\Delta t \mu^f}{2} \sum_{k=1}^{n+1} \int_{\Omega} \mathbf{D}\mathbf{u}_k : \mathbf{D}\mathbf{u}_k d\mathbf{x} \\ & \leq \frac{\rho^f}{2} \int_{\Omega} |\mathbf{u}_n|^2 d\mathbf{x} + \frac{\rho^\delta}{2} \int_{\Omega_{\mathbf{x}}^s} |\mathbf{u}_n|^2 d\mathbf{X} + \int_{\Omega_{\mathbf{x}}^s} \Psi(\mathbf{F}_n) d\mathbf{X} \\ & + \frac{\Delta t \mu^f}{2} \sum_{k=1}^n \int_{\Omega} \mathbf{D}\mathbf{u}_k : \mathbf{D}\mathbf{u}_k d\mathbf{x} + R_{n+1}, \end{aligned} \quad (28)$$

where R_{n+1} is defined in equation (26).

Proof. Let $\mathbf{v} = \mathbf{u}_{n+1}$ in (15) and multiply Δt on both side of the equation, and then let $q = p_{n+1}$ in (16) and substitute into equation (15), we get:

$$\begin{aligned} & \rho^f \int_{\Omega} (\mathbf{u}_{n+1} - \mathbf{u}_n) \cdot \mathbf{u}_{n+1} d\mathbf{x} + \frac{\Delta t \mu^f}{2} \int_{\Omega} \mathbf{D}\mathbf{u}_{n+1} : \mathbf{D}\mathbf{u}_{n+1} d\mathbf{x} \\ & + \rho^\delta \int_{\Omega_{\mathbf{x}}^s} (\mathbf{u}_{n+1} - \mathbf{u}_n) \cdot \mathbf{u}_{n+1} d\mathbf{X} \\ & + c_1 \Delta t \int_{\Omega_{\mathbf{x}}^s} \mathbf{F}_{n+1} : \nabla_{\mathbf{x}} \mathbf{u}_{n+1} d\mathbf{X} - c_1 \Delta t \int_{\Omega_{n+1}^s} \nabla \cdot \mathbf{u}_{n+1} d\mathbf{x} = 0. \end{aligned} \quad (29)$$

Using the Cauchy-Schwarz inequality and the fact $ab \leq \frac{a^2+b^2}{2}$, we have:

$$\int_{\omega} \mathbf{u}_n \cdot \mathbf{u}_{n+1} d\mathbf{x} \leq \|\mathbf{u}_n\|_{0,\omega} \|\mathbf{u}_{n+1}\|_{0,\omega} \leq \frac{\|\mathbf{u}_n\|_{0,\omega}^2 + \|\mathbf{u}_{n+1}\|_{0,\omega}^2}{2},$$

125 where $\omega = \Omega$ or Ω_{n+1}^s . Substituting the above relation into (29), we get (28) due to Proposition 8 and Lemma 9. \square

Remark 6. *Relation (28) does not exactly show energy nonincreasing, because we do not know whether R_{n+1} is greater or less than 0. However, R_{n+1} is $O(\Delta t^2)$ and this will be demonstrated in section 7 by numerical tests. In order to test the energy property, let us use the following notation for the different contributions to the total energy in (28): (1) Kinetic energy of fluid*

plus fictitious fluid $E_k(\Omega) = \frac{\rho^f}{2} \int_{\Omega} |\mathbf{u}_n|^2 d\mathbf{x}$; (2) Kinetic energy of solid minus fictitious fluid $E_k(\Omega_{\mathbf{X}}^s) = \frac{\rho^s}{2} \int_{\Omega_{\mathbf{X}}^s} |\mathbf{u}_n|^2 d\mathbf{X}$; (3) Viscous dissipation $E_d(\Omega) = \frac{\Delta t \mu^f}{2} \sum_{k=0}^n \int_{\Omega} \mathbf{D}\mathbf{u}_k : \mathbf{D}\mathbf{u}_k d\mathbf{x}$; (4) Potential energy of the solid $E_p(\Omega_{\mathbf{X}}^s) = \int_{\Omega_{\mathbf{X}}^s} \Psi(\mathbf{F}_n) d\mathbf{X}$. Denote the total energy as $E_{total} = E_k(\Omega) + E_k(\Omega_{\mathbf{X}}^s) + E_d(\Omega) + E_p(\Omega_{\mathbf{X}}^s)$, and the energy ratio as:

$$E_{ratio} = \frac{E_{total}(t_n)}{E_{total}(t_0)}. \quad (30)$$

We shall numerically demonstrate that E_{ratio} is nonincreasing in section 7.

6. Discretization in space

We shall use a fixed Eulerian mesh for Ω and an updated Lagrangian mesh for Ω_{n+1}^s to discretize Problem 2. First, we discretize Ω as Ω^h with the corresponding finite element spaces as

$$V^h(\Omega^h) = \text{span} \{\varphi_1, \dots, \varphi_{N^u}\} \subset H_0^1(\Omega)$$

and

$$L^h(\Omega^h) = \text{span} \{\phi_1, \dots, \phi_{N^p}\} \subset L_0^2(\Omega).$$

The approximated solution \mathbf{u}^h and p^h can be expressed in terms of these basis functions as

$$\mathbf{u}^h(\mathbf{x}) = \sum_{i=1}^{N^u} \mathbf{u}(\mathbf{x}_i) \varphi_i(\mathbf{x}), \quad p^h(\mathbf{x}) = \sum_{i=1}^{N^p} p(\mathbf{x}_i) \phi_i(\mathbf{x}). \quad (31)$$

We further discretize Ω_0^s as Ω_0^{sh} with the corresponding finite element spaces as:

$$V^{sh}(\Omega_0^{sh}) = \text{span} \{\varphi_1^s, \dots, \varphi_{N^s}^s\} \subset H^1(\Omega_0^s),$$

then move the vertices of each element of Ω_n^{sh} by their own velocities to get Ω_{n+1}^{sh} , and approximate $\mathbf{u}^h(\mathbf{x})|_{\mathbf{x} \in \Omega_{n+1}^{sh}}$ as:

$$\mathbf{u}^{sh}(\mathbf{x}) = \sum_{i=1}^{N^s} \mathbf{u}^h(\mathbf{x}_i^s) \varphi_i^s(\mathbf{x}) = \sum_{i=1}^{N^s} \sum_{j=1}^{N^u} \mathbf{u}(\mathbf{x}_j) \varphi_j(\mathbf{x}_i^s) \varphi_i^s(\mathbf{x}), \quad (32)$$

where \mathbf{x}_i^s is the nodal coordinate of the solid mesh. Notice that the above approximation defines an L^2 projection P_{n+1} from $V^h(\Omega^h)^d$ to $V^{sh}(\Omega_{n+1}^{sh})^d$: $P_{n+1}(\mathbf{u}^h(\mathbf{x})) = \mathbf{u}^{sh}(\mathbf{x})$,

We then discretize Problem 2 in space as follows.

Problem 11. Given \mathbf{u}_n^h, p_n^h and Ω_n^{sh} , find $\mathbf{u}_{n+1}^h \in V^h(\Omega^h)^d, p_{n+1}^h \in L^h(\Omega^h)$ and Ω_{n+1}^{sh} , such that for $\forall \mathbf{v} \in V^h(\Omega^h)^d, \forall q \in L^h(\Omega^h)$, the following four relations

hold:

$$\begin{aligned}
& \rho^f \int_{\Omega^h} \frac{\mathbf{u}_{n+1}^h - \mathbf{u}_n^h}{\Delta t} \cdot \mathbf{v} d\mathbf{x} + \rho^f \int_{\Omega^h} (\mathbf{u}_{n+1}^h \cdot \nabla) \mathbf{u}_{n+1}^h \cdot \mathbf{v} d\mathbf{x} \\
& + \frac{\mu^f}{2} \int_{\Omega^h} \mathbf{D}\mathbf{u}_{n+1}^h : \mathbf{D}\mathbf{v} d\mathbf{x} - \int_{\Omega^h} p_{n+1}^h \nabla \cdot \mathbf{v} d\mathbf{x} \\
& + \rho^\delta \int_{\Omega_{\mathbf{x}}^{sh}} \frac{\mathbf{u}_{n+1}^{sh} - \mathbf{u}_n^{sh}}{\Delta t} \cdot \mathbf{v}^s d\mathbf{X} + c_1 \Delta t \int_{\Omega_{\mathbf{x}}^{sh}} \nabla_{\mathbf{X}} \mathbf{u}_{n+1}^{sh} : \nabla_{\mathbf{X}} \mathbf{v}^s d\mathbf{X} \\
& - c_1 \int_{\Omega_{n+1}^{sh}} J_{n+1}^{-1} \nabla \cdot \mathbf{v}^s d\mathbf{x} = -c_1 \int_{\Omega_{\mathbf{x}}^{sh}} \mathbf{F}_n^{sh} : \nabla_{\mathbf{X}} \mathbf{v}^s d\mathbf{X}, \\
& \qquad \qquad \qquad - \int_{\Omega} q \nabla \cdot \mathbf{u}_{n+1}^h d\mathbf{x} = 0,
\end{aligned} \tag{33}$$

$$\Omega_{n+1}^{sh} = \{ \mathbf{x} : \mathbf{x} = \mathbf{x}_n + \Delta t \mathbf{u}_{n+1}^{sh}, \mathbf{x}_n \in \Omega_n^{sh} \}, \tag{35}$$

and

$$\mathbf{F}_{n+1}^{sh} = \mathbf{F}_n^{sh} + \Delta t \nabla_{\mathbf{X}} \mathbf{u}_{n+1}^{sh}, \tag{36}$$

where $\mathbf{u}^{sh} = P_{n+1}(\mathbf{u}^h)$ and $\mathbf{v}^s = P_{n+1}(\mathbf{v})$.

Remark 7. The proof of the energy estimate (Proposition 10) for the spatially
135 continuous case can also be applied to the discrete case (see Appendix A).

Remark 8. There are two sources of nonlinearity in Problem 11: the convection
term and the moving solid domain. We can accommodate these by moving the
convection term to the right-hand side of the equation, and using a fixed-point
iteration to construct Ω_{n+1}^s in order to solve the nonlinear system at each time
140 step. For other methods to treat convection, readers may refer to [25, 26]. We
shall only use this fully implicit implementation to consider low Reynolds number
($Re \approx 50$) cases in this paper in order to test the energy stability.

Remark 9. A two-step explicit splitting scheme (\mathbf{F} -scheme) is discussed in
Appendix B with corresponding energy analysis. This scheme is similar to that
145 in [22] (σ -scheme), which may be adapted to problems at large Reynolds number
(see [22] for more examples).

7. Numerical experiments

In this section, we focus on validation of the energy stability of the proposed
numerical method in two and three dimensions. For more two-dimensional nu-
150 merical examples and validation of the basic algorithm see [22]. We shall use
linear triangles (2D) or linear tetrahedra (3D) to discretize the solid domain
 Ω_0^s . In domain Ω , the $P_2/(P_1 + P_0)$ elements will be used, i.e., the standard
Taylor-Hood element P_2P_1 is enriched by a constant P_0 for approximation of
the pressure. This element has the property of local mass conservation and the
155 constant P_0 may better capture the element-based jump of pressure [27, 28]. We

shall demonstrate the improvement of mass conservation and energy conservation by using the $P_2/(P_1 + P_0)$ elements compared to the P_2P_1 elements. We shall also validate that the total energy is nonincreasing as stated in Proposition 10 and Remark 6.

160 *7.1. Oscillating disc driven by an initial kinetic energy (activated disc)*

In this test, we consider an enclosed flow ($\mathbf{n} \cdot \mathbf{u} = 0$) in $\Omega = [0, 1] \times [0, 1]$ with a periodic boundary condition. A solid disc is initially located in the middle of the square Ω and has a radius of 0.2. The initial velocity of the fluid and solid are prescribed by the following stream function

$$\Psi = \Psi_0 \sin(ax) \sin(by),$$

where $\Psi_0 = 5.0 \times 10^{-2}$ and $a = b = 2\pi$. In this test, $\rho^f = 1$, $\mu^f = 0.01$, $\rho^s = 1.5$ and $c_1 = 1$. In order to visualize the flow a snapshot of the velocity and deformation fields is presented in Figure 2, and the evolution of energy is presented in Figure 3 using a 50×50 mesh (biquadratic squares for the fluid velocity and 3052 bilinear triangles for the solid velocity).

165

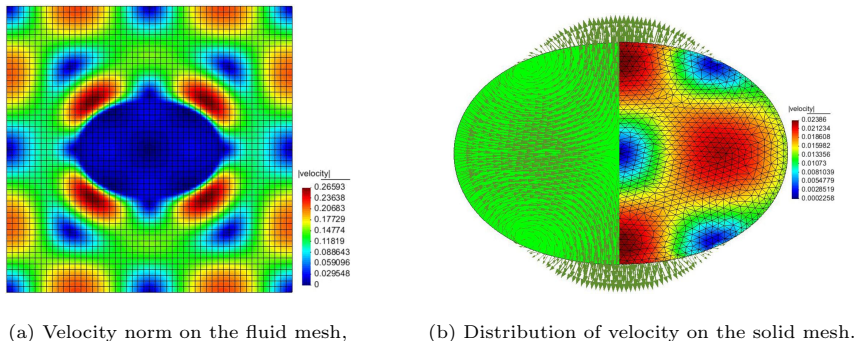


Figure 2: Snapshot at $t = 0.25$, $\Delta t = 5.0 \times 10^{-3}$.

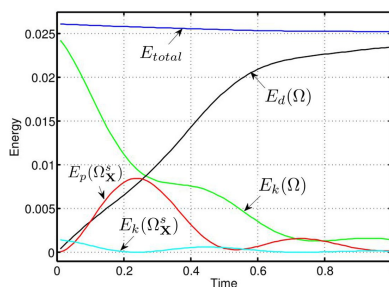


Figure 3: Evolution of energy, $\Delta t = 5.0 \times 10^{-3}$.

We commence by comparing P_2/P_1 elements and $P_2/(P_1 + P_0)$ elements. The evolution of mass variation and energy ratio are demonstrated in Figure 4,

from which it can be seen that the enrichment of the pressure field by a constant P_0 has an effect of stabilizing the mass and energy evolution. In addition, this enrichment of the pressure field dramatically improves the mass conservation, although the effect for energy conservation is not obvious. Then using element $P_2/(P_1 + P_0)$, time convergence of the total energy can be observed from Figure 5 (a), from which we can see a nonincreasing energy and a first order time convergence for both the implicit and explicit scheme (see Appendix B for the energy estimate of the explicit scheme). It can be seen from Figure 5 (b) that the residual term defined in (26) is very small and converges rapidly to zero when reducing Δt ($\sim O(\Delta t^2)$).

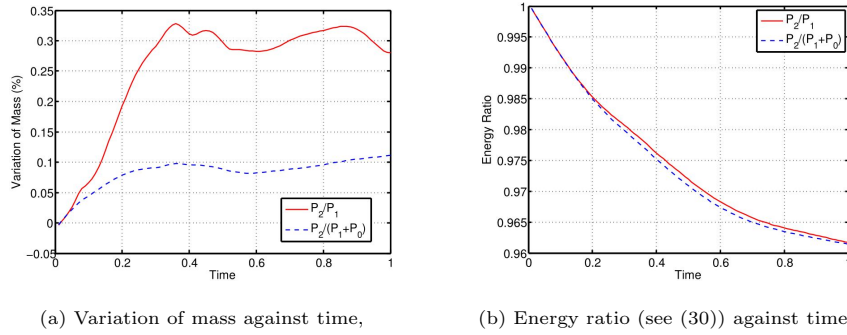


Figure 4: Variation of mass and energy, $\Delta t = 5.0 \times 10^{-3}$.

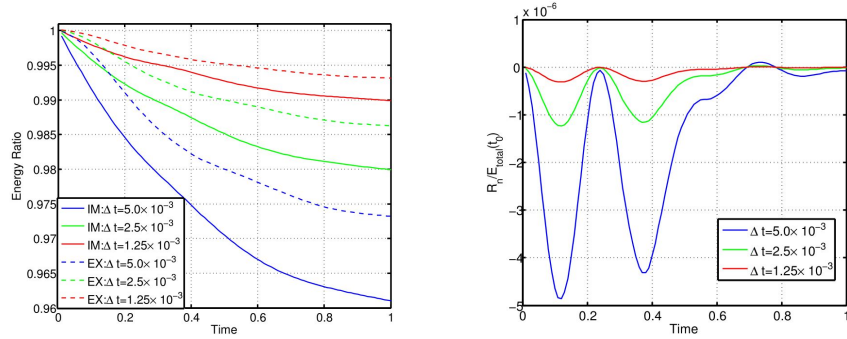


Figure 5: Evolution of the energy ratio and residual R_n for the test problem of activated disc.

7.2. Oscillating disc driven by an initial potential energy (stretched disc)

In the previous example, the disc oscillates because a kinetic energy is prescribed for the FSI system at the beginning. In this test, we shall stretch the disc and create a potential energy in the solid, then release it causing the disc to oscillate due to this potential energy. The computational domain is a square

$\Omega = [0, 1] \times [0, 1]$. One quarter of a solid disc is located in the left-bottom corner of the square, and initially stretched as an ellipse as shown in Figure 6. Notice
 185 the equation of an ellipse $\frac{x^2}{a^2} + \frac{y^2}{b^2} = 1$ and its area πab , hence we ensure that this stretch does not change mass of the solid.

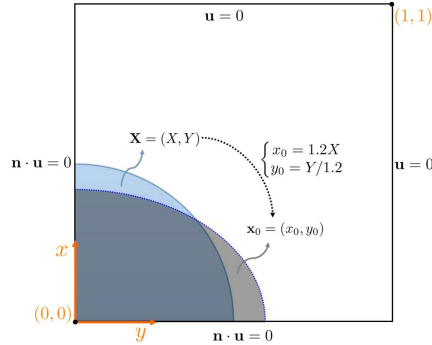
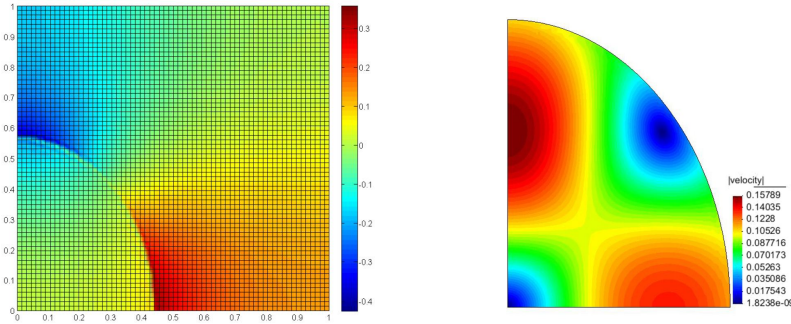


Figure 6: Computational domain and boundary conditions for test problem 7.2 (stretched disc).

We choose $\rho^f = 1$, $\mu^f = 0.01$, $\rho^s = 2$ and $c_1 = 2$. The fluid adopts a mesh of 66×66 biquadratic squares, and the solid has similar node density (8206 linear triangles) as the fluid. A snapshot of pressure on the fluid mesh and corresponding solid deformation with its velocity norm are displayed in Figure 7, and the evolution of energy is presented in Figure 8. The nonincreasing total
 190 energy can be observed from Figure 9 (a) for both the implicit and explicit scheme (see Appendix B for energy estimate of the explicit scheme). It can be seen from Figure 9 (b) that the residual term defined in (26) is very small and
 195 converges rapidly to zero when reducing Δt .



(a) Distribution of pressures on the fluid mesh, (b) velocity norm on the solid.

Figure 7: A snapshot at $t = 1$, $\Delta t = 5.0 \times 10^{-3}$.

7.3. Oscillating ball driven by an initial kinetic energy

In this section, we consider a 3D oscillating ball, which is an extension of the example in section 7.1. The ball is initially located at the center of

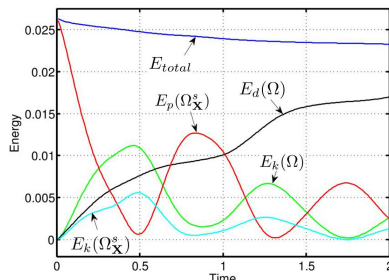
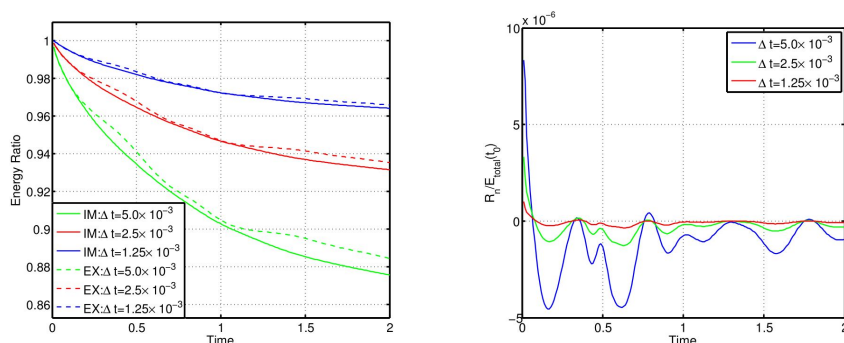


Figure 8: Evolution of energy, $\Delta t = 5.0 \times 10^{-3}$.



(a) Energy ratio against time (defined in (30)), (b) $R_n/E_{total}(t_0)$ against time (defined in (26)).

Figure 9: Evolution of the energy ratio and residual R_n for the test problem of stretched disc.

200 $\Omega = [0, 1] \times [0, 1] \times [0, 0.6]$ with a radius of 0.2. Using the property of symmetry
 this computation is carried out on 1/8 of domain Ω : $[0, 0.5] \times [0, 0.5] \times [0, 0.3]$.
 The initial velocities of x and y components are the same as that used in section
 7.1 and the z component is set to be 0 at the beginning. We adopt the same
 parameter and mesh size defined in section 7.1 (with the same mesh size in
 205 the z direction). A snapshot of the 1/8 solid ball and the corresponding fluid
 velocity norm are presented in Figure 10, and the nonincreasing energy property
 is presented in Figure 11.

8. Conclusions

In this article, we first introduce an implicit version of [22] for the one-
 field fictitious domain method (one-field FDM) based upon updating the solid
 210 deformation tensor \mathbf{F} . Then the energy-preserving property for this one-field
 FDM is proved on the continuous level, and the energy-nonincreasing property
 is proved after discretization in time and space. The energy property for an
 explicit scheme is also analyzed in Appendix B. Finally, a selection of numerical
 tests are presented to demonstrate this theoretical energy estimate in both two
 215 and three dimensions. It has therefore been demonstrated that the proposed

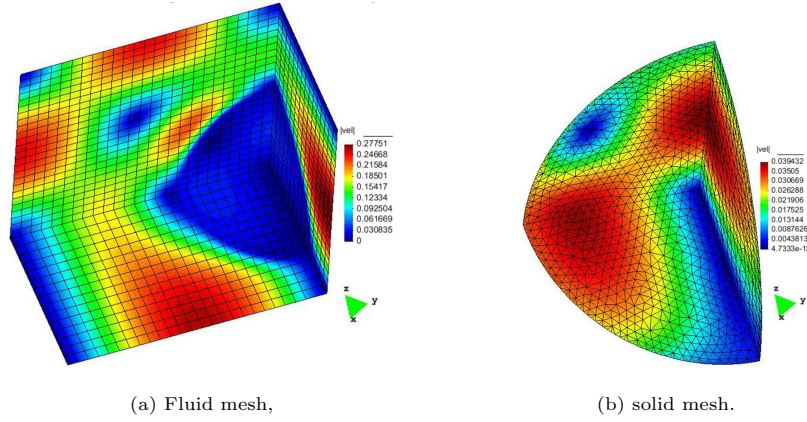


Figure 10: Velocity norm at $t = 0.2$.

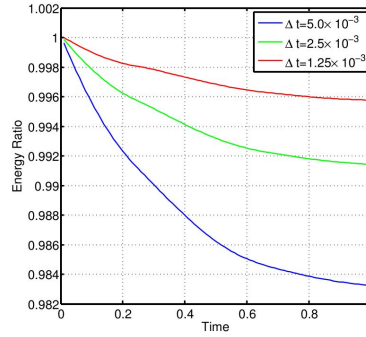


Figure 11: Evolution of the energy ratio (defined in (30)) for the test problem of oscillating ball.

one-field FDM is a stable, robust and computationally efficient technique for the solution of a wide range of fluid-structure interaction problems.

Appendix A. Stability analysis after space discretization

As with the previous stability estimate (Proposition 10) after time discretization, we have the following estimate after space discretization.

Proposition 12. *Let $(\mathbf{u}_{n+1}^h, p_{n+1}^h)$ be the solution pair of Problem 11. If $\rho^\delta \geq 0$,*

then

$$\begin{aligned}
& \frac{\rho^f}{2} \int_{\Omega^h} |\mathbf{u}_{n+1}^h|^2 d\mathbf{x} + \frac{\rho^\delta}{2} \int_{\Omega_{\mathbf{x}}^{sh}} |\mathbf{u}_{n+1}^{sh}|^2 d\mathbf{X} + \int_{\Omega_{\mathbf{x}}^{sh}} \Psi(\mathbf{F}_{n+1}^{sh}) d\mathbf{X} \\
& + \frac{\Delta t \mu^f}{2} \sum_{k=1}^{n+1} \int_{\Omega^h} \mathbf{D}\mathbf{u}_k^h : \mathbf{D}\mathbf{u}_k^h d\mathbf{x} \\
& \leq \frac{\rho^f}{2} \int_{\Omega^h} |\mathbf{u}_n^h|^2 d\mathbf{x} + \frac{\rho^\delta}{2} \int_{\Omega_{\mathbf{x}}^{sh}} |\mathbf{u}_n^{sh}|^2 d\mathbf{X} + \int_{\Omega_{\mathbf{x}}^{sh}} \Psi(\mathbf{F}_n^{sh}) d\mathbf{X} \\
& + \frac{\Delta t \mu^f}{2} \sum_{k=1}^n \int_{\Omega^h} \mathbf{D}\mathbf{u}_k^h : \mathbf{D}\mathbf{u}_k^h d\mathbf{x} + R_{n+1}^h,
\end{aligned} \tag{A.1}$$

where

$$R_{n+1}^h = \frac{c_1 \Delta t^2}{2} \int_{\Omega_{\mathbf{x}}^{sh}} \left(\left| (\mathbf{F}_{n+1}^{sh})^{-1} \nabla_{\mathbf{x}} \mathbf{u}_{n+1}^{sh} \right|^2 - |\nabla_{\mathbf{x}} \mathbf{u}_{n+1}^{sh}|^2 \right) d\mathbf{X}. \tag{A.2}$$

Proof. Let $\mathbf{v} = \mathbf{u}_{n+1}^h$ in (33) and multiply Δt on both side of the equation, and then let $q = p_{n+1}^h$ in (34) and substitute into equation (33), we get:

$$\begin{aligned}
& \rho^f \int_{\Omega^h} (\mathbf{u}_{n+1}^h - \mathbf{u}_n^h) \cdot \mathbf{u}_{n+1}^h d\mathbf{x} + \frac{\Delta t \mu^f}{2} \int_{\Omega^h} \mathbf{D}\mathbf{u}_{n+1}^h : \mathbf{D}\mathbf{u}_{n+1}^h d\mathbf{x} \\
& + \rho^\delta \int_{\Omega_{\mathbf{x}}^{sh}} (\mathbf{u}_{n+1}^{sh} - \mathbf{u}_n^{sh}) \cdot \mathbf{u}_{n+1}^{sh} d\mathbf{X} \\
& + c_1 \Delta t \int_{\Omega_{\mathbf{x}}^{sh}} \mathbf{F}_{n+1}^{sh} : \nabla_{\mathbf{x}} \mathbf{u}_{n+1}^{sh} d\mathbf{X} - c_1 \Delta t \int_{\Omega_{n+1}^{sh}} \nabla \cdot \mathbf{u}_{n+1}^{sh} d\mathbf{x} = 0.
\end{aligned} \tag{A.3}$$

Using the Cauchy-Schwarz inequality and the fact $ab \leq \frac{a^2+b^2}{2}$, we have:

$$\int_{\omega} \mathbf{u}_n \cdot \mathbf{u}_{n+1} d\mathbf{x} \leq \|\mathbf{u}_n\|_{0,\omega} \|\mathbf{u}_{n+1}\|_{0,\omega} \leq \frac{\|\mathbf{u}_n\|_{0,\omega}^2 + \|\mathbf{u}_{n+1}\|_{0,\omega}^2}{2},$$

where $\omega = \Omega^h$ or Ω_{n+1}^{sh} . Notice that Lemma 6 to 9 still hold after space discretization, then substituting the above relation into (A.3) gives (A.1). \square

Appendix B. Energy estimate for a two-step explicit splitting scheme

In this section, we analyze the energy property for the 2-step explicit splitting scheme introduced in [22], which can be stated as follows (corresponding to the implicit Problem 11):

Problem 13. Given \mathbf{u}_n^h , p_n^h and Ω_n^{sh} , find $\mathbf{u}_{n+1}^h \in V^h(\Omega^h)^d$, $p_{n+1}^h \in L^h(\Omega^h)$ and Ω_{n+1}^{sh} , such that for $\forall \mathbf{v} \in V^h(\Omega^h)^d$, $\forall q \in L^h(\Omega^h)$, the following 5 relations hold:

(1) convection step:

$$\rho^f \int_{\Omega^h} \frac{\mathbf{u}_{n+1/2}^h - \mathbf{u}_n^h}{\Delta t} \cdot \mathbf{v} d\mathbf{x} + \rho^f \int_{\Omega^h} \left(\mathbf{u}_{n+1/2}^h \cdot \nabla \right) \mathbf{u}_{n+1/2}^h \cdot \mathbf{v} d\mathbf{x} = 0, \quad (\text{B.1})$$

(2) diffusion step:

$$\begin{aligned} & \rho^f \int_{\Omega^h} \frac{\mathbf{u}_{n+1}^h - \mathbf{u}_{n+1/2}^h}{\Delta t} \cdot \mathbf{v} d\mathbf{x} + \frac{\mu^f}{2} \int_{\Omega^h} \text{Du}_{n+1}^h : \text{Dv} d\mathbf{x} \\ & - \int_{\Omega^h} p_{n+1}^h \nabla \cdot \mathbf{v} d\mathbf{x} + \rho^\delta \int_{\Omega_{\mathbf{x}}^{sh}} \frac{\mathbf{u}_{n+1}^{sh} - \mathbf{u}_n^{sh}}{\Delta t} \cdot \mathbf{v}^s d\mathbf{X} \\ & + c_1 \Delta t \int_{\Omega_{\mathbf{x}}^{sh}} \nabla_{\mathbf{X}} \mathbf{u}_{n+1}^{sh} : \nabla_{\mathbf{X}} \mathbf{v}^s d\mathbf{X} - c_1 \int_{\Omega_n^{sh}} J_n^{-1} \nabla_n \cdot \mathbf{v}^s d\mathbf{x} \\ & = -c_1 \int_{\Omega_{\mathbf{x}}^{sh}} \mathbf{F}_n^{sh} : \nabla_{\mathbf{X}} \mathbf{v}^s d\mathbf{X}, \end{aligned} \quad (\text{B.2})$$

$$- \int_{\Omega} q \nabla \cdot \mathbf{u}_{n+1}^h d\mathbf{x} = 0, \quad (\text{B.3})$$

$$\Omega_{n+1}^{sh} = \{ \mathbf{x} : \mathbf{x} = \mathbf{x}_n + \Delta t \mathbf{u}_{n+1}^{sh}, \mathbf{x}_n \in \Omega_n^{sh} \}, \quad (\text{B.4})$$

and

$$\mathbf{F}_{n+1}^{sh} = \mathbf{F}_n^{sh} + \Delta t \nabla_{\mathbf{X}} \mathbf{u}_{n+1}^{sh}, \quad (\text{B.5})$$

230 where $\mathbf{u}^{sh} = P_{n+1}(\mathbf{u}^h)$, $\mathbf{v}^s = P_{n+1}(\mathbf{v})$, and $\nabla_n(\cdot) = \frac{\partial(\cdot)}{\partial \mathbf{x}_n}$.

As with the previous analysis for the implicit scheme, if we let $\mathbf{v} = \mathbf{u}_{n+1}^h$ in equations (B.1), (B.2) and (B.3), adding up these three equations, using (B.5) and $\mathbf{u}^{sh} = P_{n+1}(\mathbf{u}^h)$, gives the energy estimate as follows.

Proposition 14. *Let $(\mathbf{u}_{n+1}, p_{n+1})$ be the solution pair of Problem 13. If $\rho^\delta \geq 0$, then*

$$\begin{aligned} & \frac{\rho^f}{2} \int_{\Omega^h} |\mathbf{u}_{n+1}^h|^2 d\mathbf{x} + \frac{\rho^\delta}{2} \int_{\Omega_{\mathbf{x}}^{sh}} |\mathbf{u}_{n+1}^h|^2 d\mathbf{X} + \int_{\Omega_{\mathbf{x}}^{sh}} \Psi(\mathbf{F}_{n+1}^{sh}) d\mathbf{X} \\ & + \frac{\Delta t \mu^f}{2} \sum_{k=1}^{n+1} \int_{\Omega^h} \text{Du}_k^h : \text{Du}_k^h d\mathbf{x} \\ & \leq \frac{\rho^f}{2} \int_{\Omega^h} |\mathbf{u}_n^h|^2 d\mathbf{x} + \frac{\rho^\delta}{2} \int_{\Omega_{\mathbf{x}}^{sh}} |\mathbf{u}_n^h|^2 d\mathbf{X} + \int_{\Omega_{\mathbf{x}}^{sh}} \Psi(\mathbf{F}_n^{sh}) d\mathbf{X} \\ & + \frac{\Delta t \mu^f}{2} \sum_{k=1}^n \int_{\Omega^h} \text{Du}_k^h : \text{Du}_k^h d\mathbf{x} + R_{n+1}^{im} + R_{n+1}^{ex} + R_{n+1}^{split}, \end{aligned} \quad (\text{B.6})$$

where $R_{n+1}^{im} = R_{n+1}^h$ as defined in (A.2).

$$R_{n+1}^{ex} = c_1 \Delta t \int_{\Omega_{\mathbf{x}}^{sh}} (\nabla_n \cdot \mathbf{u}_{n+1}^{sh} - \nabla \cdot \mathbf{u}_{n+1}^h) d\mathbf{X}, \quad (\text{B.7})$$

and

$$R_{n+1}^{split} = -\Delta t \rho^f \int_{\Omega^h} \left(\mathbf{u}_{n+1/2}^h \cdot \nabla \right) \mathbf{u}_{n+1/2}^h \cdot \mathbf{u}_{n+1}^h d\mathbf{x}. \quad (\text{B.8})$$

References

- 235 [1] J. Degroote, K.-J. Bathe, J. Vierendeels, Performance of a new partitioned procedure versus a monolithic procedure in fluid–structure interaction, *Computers & Structures* 87 (11-12) (2009) 793–801. doi:10.1016/j.compstruc.2008.11.013.
- 240 [2] U. Küttler, W. A. Wall, Fixed-point fluid–structure interaction solvers with dynamic relaxation, *Computational Mechanics* 43 (1) (2008) 61–72. doi:10.1007/s00466-008-0255-5.
- 245 [3] M. Heil, An efficient solver for the fully coupled solution of large-displacement fluid–structure interaction problems, *Computer Methods in Applied Mechanics and Engineering* 193 (1-2) (2004) 1–23. doi:10.1016/j.cma.2003.09.006.
- [4] M. Heil, A. L. Hazel, J. Boyle, Solvers for large-displacement fluid–structure interaction problems: segregated versus monolithic approaches, *Computational Mechanics* 43 (1) (2008) 91–101. doi:10.1007/s00466-008-0270-6.
- 250 [5] R. L. Muddle, M. Mihajlović, M. Heil, An efficient preconditioner for monolithically-coupled large-displacement fluid–structure interaction problems with pseudo-solid mesh updates, *Journal of Computational Physics* 231 (21) (2012) 7315–7334. doi:10.1016/j.jcp.2012.07.001.
- 255 [6] D. Boffi, N. Cavallini, L. Gastaldi, The finite element immersed boundary method with distributed lagrange multiplier, *SIAM Journal on Numerical Analysis* 53 (6) (2015) 2584–2604. doi:10.1137/140978399.
- [7] C. S. Peskin, The immersed boundary method, *Acta numerica* 11 (2002) 479–517. doi:10.1016/j.cma.2015.12.023.
- 260 [8] X. Wang, C. Wang, L. T. Zhang, Semi-implicit formulation of the immersed finite element method, *Computational Mechanics* 49 (4) (2011) 421–430. doi:10.1007/s00466-011-0652-z.
- [9] X. Wang, L. T. Zhang, Interpolation functions in the immersed boundary and finite element methods, *Computational Mechanics* 45 (4) (2009) 321–334. doi:10.1007/s00466-009-0449-5.
- 265 [10] X. Wang, L. T. Zhang, Modified immersed finite element method for fully-coupled fluid–structure interactions, *Computer Methods in Applied Mechanics and Engineering* 267 (2013) 150–169. doi:10.1016/j.cma.2013.07.019.

- [11] L. Zhang, M. Gay, Immersed finite element method for fluid-structure interactions, *Journal of Fluids and Structures* 23 (6) (2007) 839–857. doi:10.1016/j.jfluidstructs.2007.01.001.
- [12] L. Zhang, A. Gerstenberger, X. Wang, W. K. Liu, Immersed finite element method, *Computer Methods in Applied Mechanics and Engineering* 193 (21) (2004) 2051–2067. doi:10.1016/j.cma.2003.12.044.
- [13] F. P. Baaijens, A fictitious domain/mortar element method for fluid-structure interaction, *International Journal for Numerical Methods in Fluids* 35 (7) (2001) 743–761. doi:10.1002/1097-0363(20010415)35:7<743::AID-FLD109>3.0.CO;2-A.
- [14] D. Boffi, L. Gastaldi, A fictitious domain approach with lagrange multiplier for fluid-structure interactions, *Numerische Mathematik* 135 (3) (2016) 711–732. doi:10.1007/s00211-016-0814-1.
- [15] R. Glowinski, T. Pan, T. Hesla, D. Joseph, J. Périaux, A fictitious domain approach to the direct numerical simulation of incompressible viscous flow past moving rigid bodies: Application to particulate flow, *Journal of Computational Physics* 169 (2) (2001) 363–426. doi:10.1006/jcph.2000.6542.
- [16] C. Hesch, A. Gil, A. A. Carreño, J. Bonet, P. Betsch, A mortar approach for fluid-structure interaction problems: Immersed strategies for deformable and rigid bodies, *Computer Methods in Applied Mechanics and Engineering* 278 (2014) 853–882. doi:10.1016/j.cma.2014.06.004.
- [17] C. Kadapa, W. Dettmer, D. Perić, A fictitious domain/distributed lagrange multiplier based fluid-structure interaction scheme with hierarchical b-spline grids, *Computer Methods in Applied Mechanics and Engineering* 301 (2016) 1–27. doi:10.1016/j.cma.2015.12.023.
- [18] Z. Yu, A DLM/FD method for fluid/flexible-body interactions, *Journal of Computational Physics* 207 (1) (2005) 1–27. doi:10.1016/j.jcp.2004.12.026.
- [19] F. Auricchio, D. Boffi, L. Gastaldi, A. Lefieux, A. Reali, A study on unfitted 1d finite element methods, *Computers & Mathematics with Applications* 68 (12) (2014) 2080–2102. doi:10.1016/j.camwa.2014.08.018.
- [20] F. Hecht, O. Pironneau, An energy stable monolithic eulerian fluid-structure finite element method, *International Journal for Numerical Methods in Fluids* doi:10.1002/flid.4388.
- [21] O. Pironneau, Numerical study of a monolithic fluid-structure formulation, in: *Variational Analysis and Aerospace Engineering*, Springer International Publishing, 2016, pp. 401–420. doi:10.1007/978-3-319-45680-5_15. URL https://doi.org/10.1007/978-3-319-45680-5_15

- [22] Y. Wang, P. K. Jimack, M. A. Walkley, A one-field monolithic fictitious domain method for fluid–structure interactions, *Computer Methods in Applied Mechanics and Engineering* 317 (2017) 1146–1168. doi:10.1016/j.cma.2017.01.023.
- 310 [23] D. Mitrovic, D. Zubrinic, *Fundamentals of applied functional analysis*, Vol. 91, CRC Press, 1997.
- [24] S. Boyd, L. Vandenberghe, Convex optimization problems, in: *Convex Optimization*, Cambridge University Press, pp. 127–214. doi:10.1017/cbo9780511804441.005.
315 URL <https://doi.org/10.1017%2Fcbo9780511804441.005>
- [25] O. Pironneau, O. Pironneau, *Finite element methods for fluids*, Wiley Chichester, 1989.
- [26] O. Zienkiewicz, *The finite element method for fluid dynamics*, 6th Edition, Elsevier BV, 2005.
- 320 [27] D. N. Arnold, F. Brezzi, B. Cockburn, L. D. Marini, Unified analysis of discontinuous galerkin methods for elliptic problems, *SIAM Journal on Numerical Analysis* 39 (5) (2002) 1749–1779. doi:10.1137/s0036142901384162.
- 325 [28] D. Boffi, N. Cavallini, F. Gardini, L. Gastaldi, Local mass conservation of stokes finite elements, *Journal of Scientific Computing* 52 (2) (2011) 383–400. doi:10.1007/s10915-011-9549-4.